

Electronic Supplementary Information (ESI)

A Microporous Cu²⁺ MOF based on a Pyridyl – Isophthalic Acid Schiff Base Ligand with High CO₂ Uptake

Andreas Kourtellaris,^a Eleni E. Moushi,^a Ioannis Spanopoulos,^b Christos Tampaxis,^{b,c} Georgia Charalambopoulou,^c Theodore A. Steriotis,^c Giannis S. Papaefstathiou,^d Pantelis N. Trikalitis^b and Anastasios J. Tasiopoulos*,^a

^a Department of Chemistry, University of Cyprus, 1678 Nicosia, Cyprus. Fax: ++357 22895451; Tel: ++357 22892765; E-mail: atasio@ucy.ac.cy

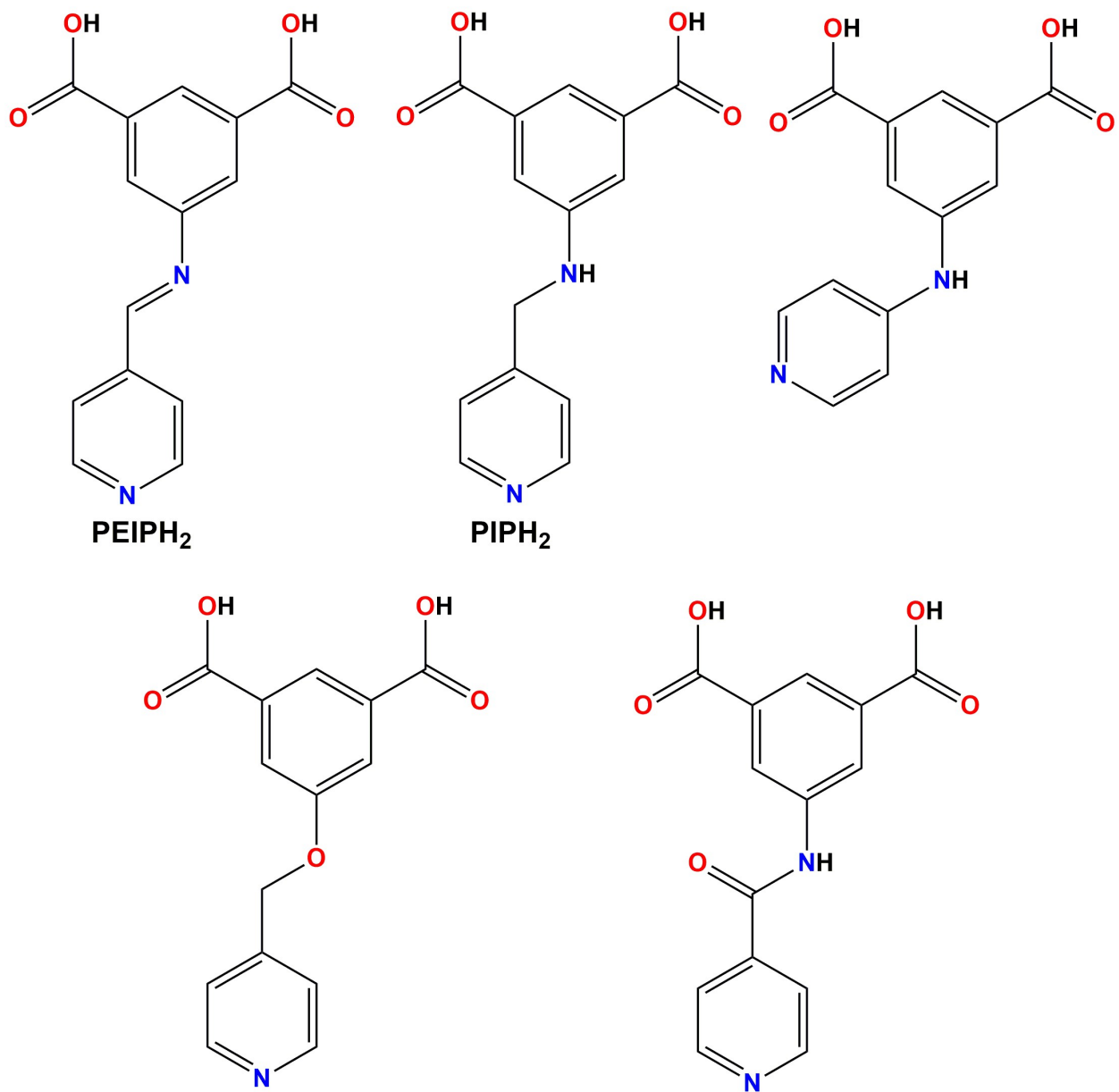
^b Department of Chemistry, University of Crete, Voutes 71003, Heraklion, Greece.

^c National Center for Scientific Research “Demokritos”, 15341 Agia Paraskevi Attikis, Greece.

^d Laboratory of Inorganic Chemistry, Department of Chemistry, National and Kapodistrian University of Athens, Panepistimiopolis Zografou 157 71, Greece.

Table of Contents

Representative Examples of Pyridyl-Isophthalic acid Ligands	S2
Powder X-ray diffraction studies	S3
IR spectra	S4
Structural figures of Cu-PEIP	S5-S6
Thermal gravimetric analyses (TGA)	S7
Gas sorption data	S8-S15
References	S16



Scheme S1. The ligands PEIPH₂ and PIPH₂ employed in this study and some representative examples of tritopic ligands consisting of a pyridyl and an isophthalic acid moieties.

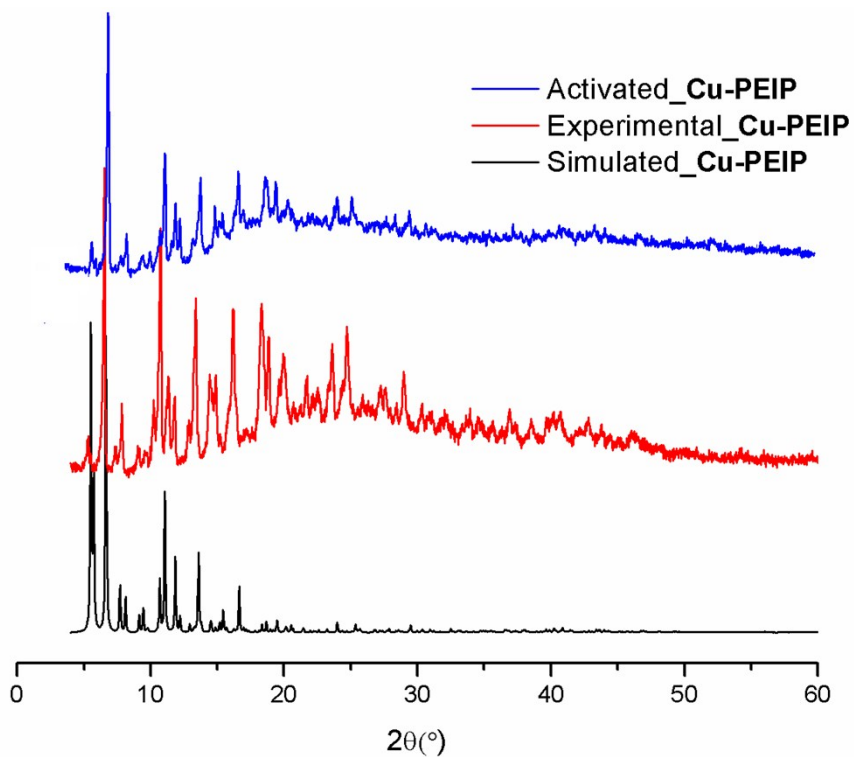


Figure S1. Power X-ray diffraction patterns for **Cu-PEIP**.

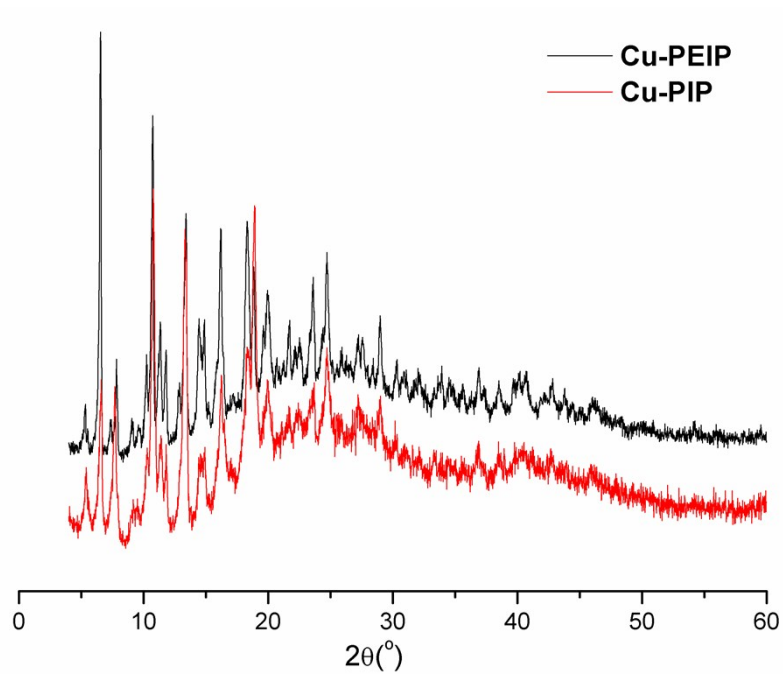


Figure S2. Power X-ray diffraction patterns (experimental) for **Cu-PEIP** and **Cu-PIP**.

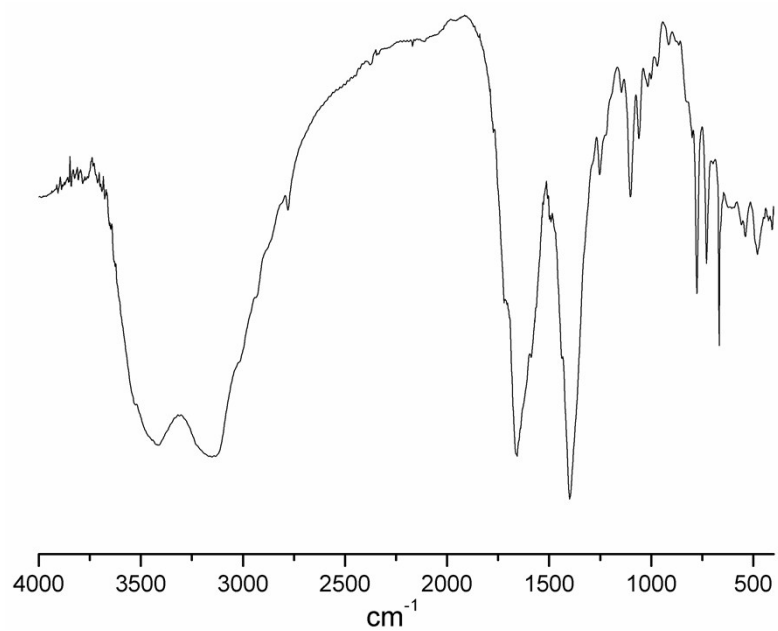


Figure S3. FTIR spectra for **Cu-PEIP**.

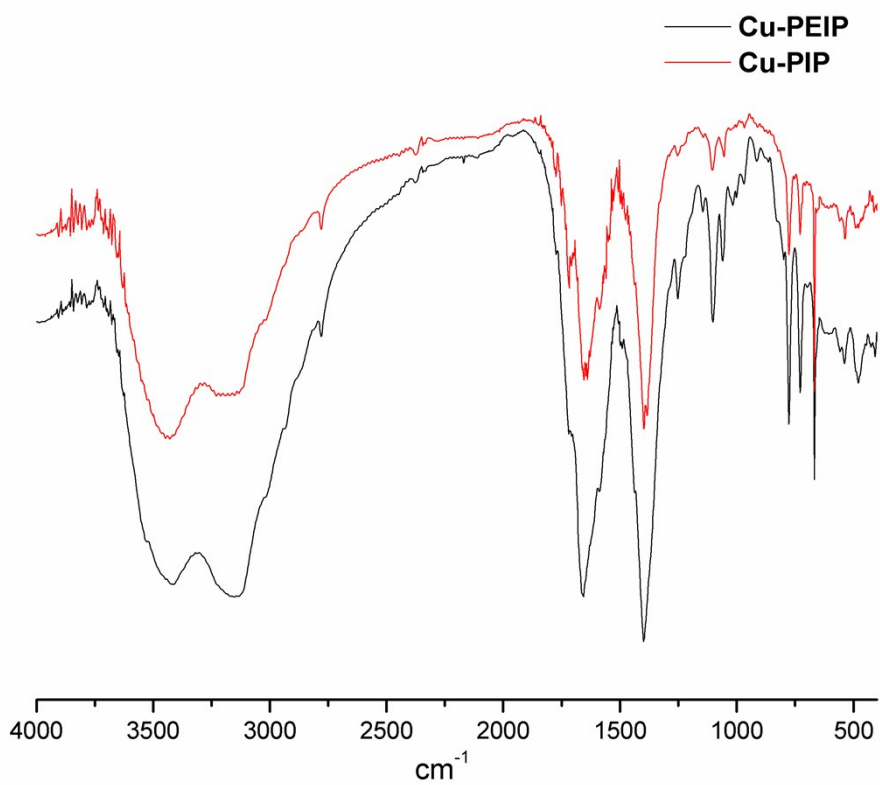


Figure S4. FTIR spectra for **Cu-PEIP** and **Cu-PIP**.

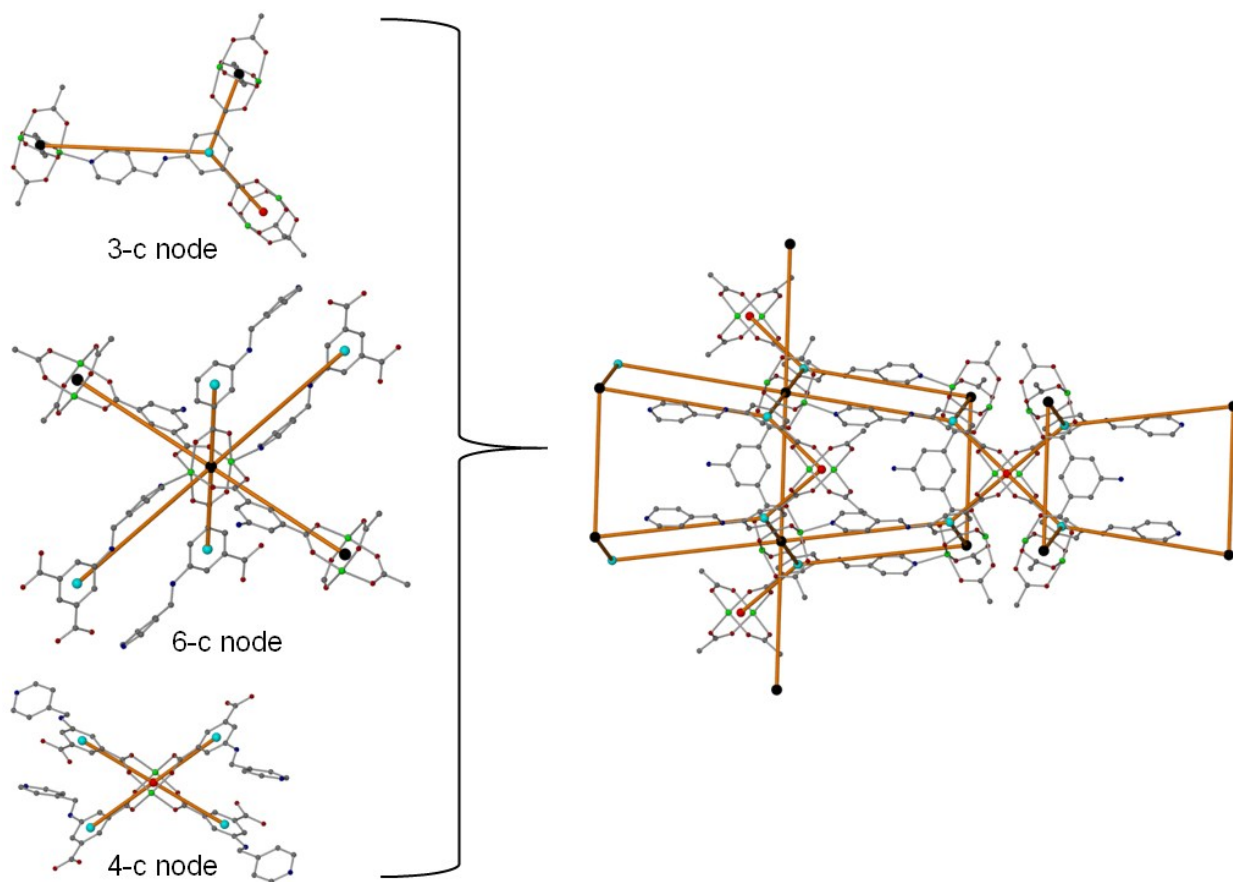


Figure S5: The deconstruction of the underline network of **Cu-PEIP**.

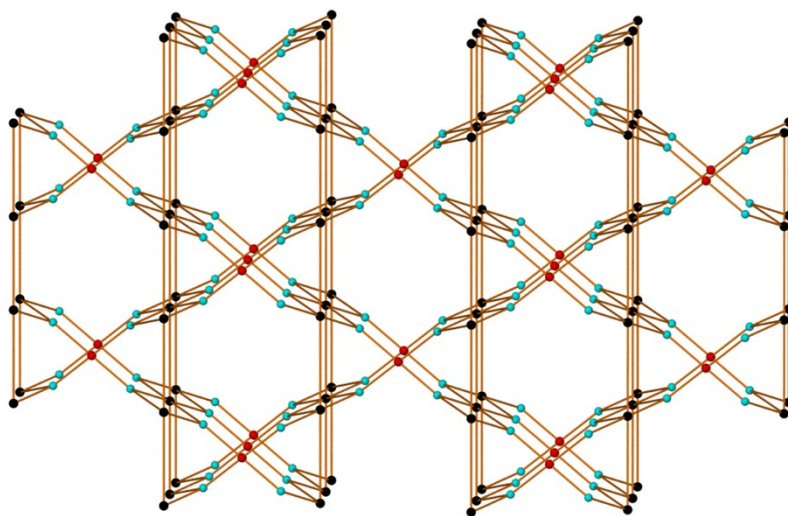


Figure S6. The trinodal net of **Cu-PEIP** down to a axis.

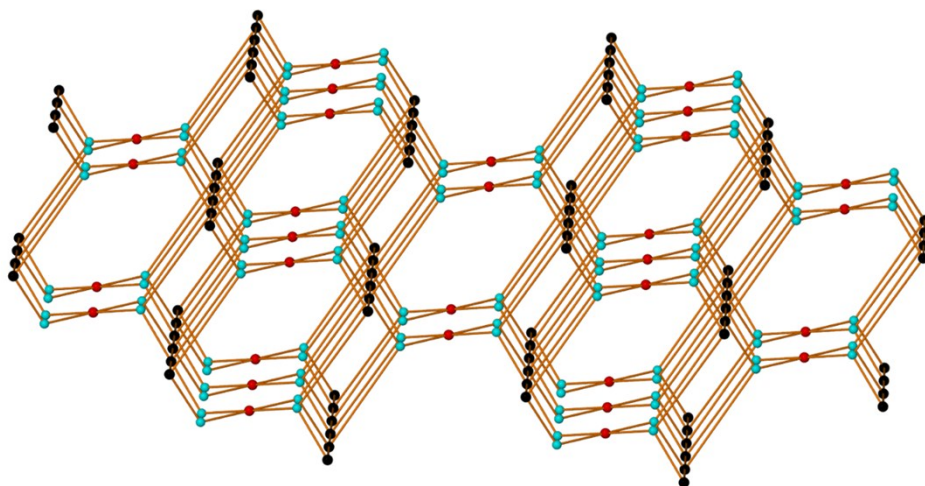


Figure S7. The trinodal net of **Cu-PEIP** down to b axis.

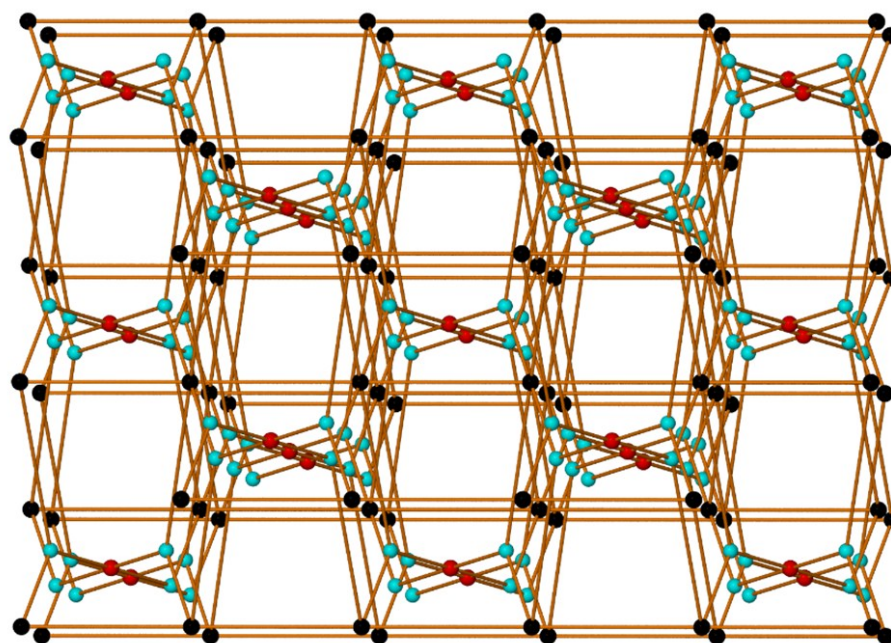


Figure S8. The trinodal net of **Cu-PEIP** down to c axis.

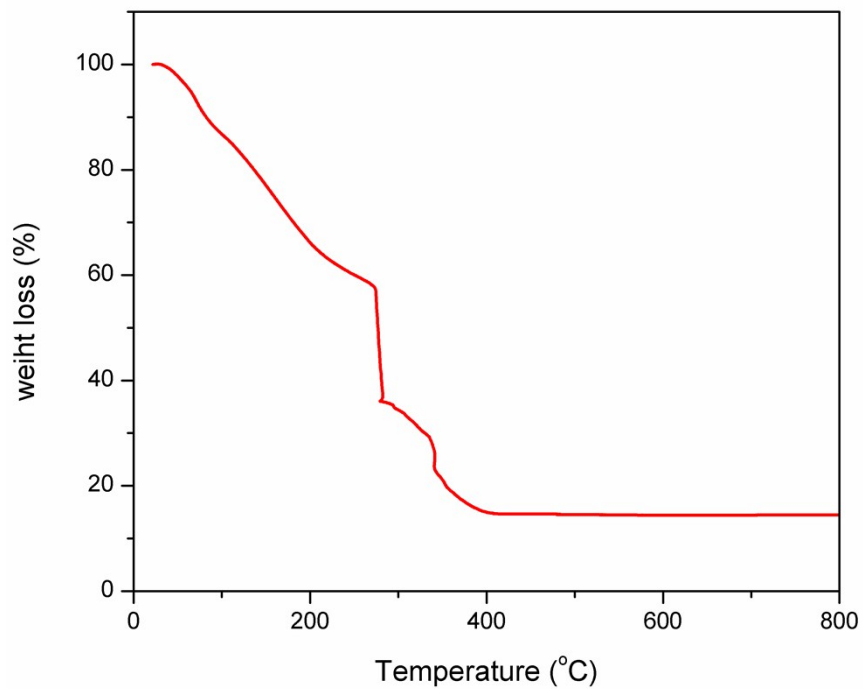


Figure S9. TGA curve of **Cu-PEIP**.

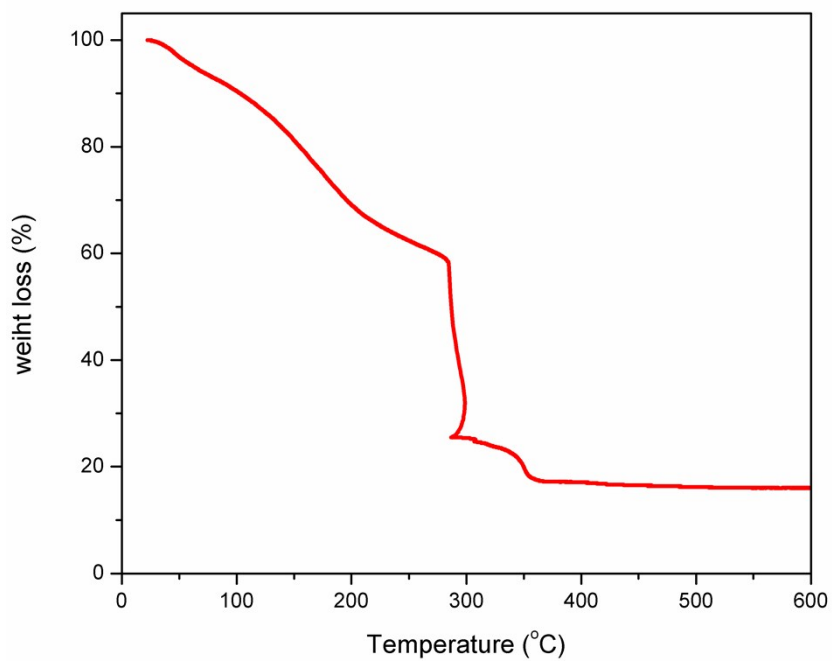


Figure S10. TGA curve of **Cu-PIP**.

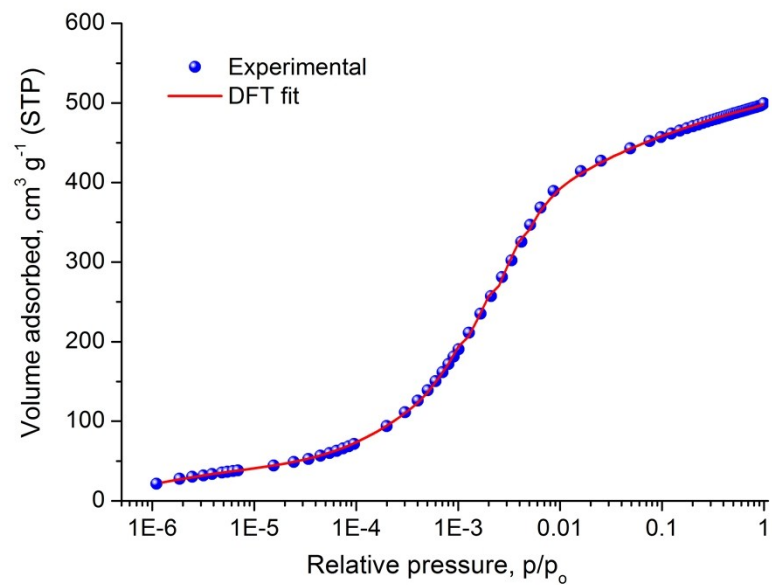


Figure S11. Argon adsorption isotherm of **Cu-PEIP** recorded at 87 K and the corresponding NLDFT fitting.

Low pressure CO₂, N₂ and CH₄ sorption isotherms, determination of heat of adsorption and selectivity (CO₂/N₂, CO₂/CH₄) calculations using IAST.

Heat of adsorption. To calculate heats of adsorptions, the corresponding adsorption isotherms at different temperatures were simultaneously fitted using the virial type¹ Equation 1:

$$\ln P = \ln N + \frac{1}{T} \sum_{i=0}^m a_i N^i + \sum_{i=0}^n b_i N^i \quad (1)$$

The heat of adsorption at zero coverage was calculated from Equation 2, where as a function of surface coverage, from Equation 3:

$$Q_{st} = -R a_0 \quad (2)$$

$$Q_{st}(N) = -R \sum_{i=0}^m a_i N^i \quad (3)$$

For the determination of the isosteric heat of adsorption using the Clausius Clapeyron equation a commercially available software, ASiQwin (version 3.01) purchased from Quantachrome, was used.

Gas selectivity using IAST. The corresponding calculations were performed according to an established procedure.² Specifically, the single-component adsorption isotherms were described by fitting the data with the following virial-type equation:

$$p = \frac{n}{K} \exp\left(\frac{c_1 n + c_2 n^2 + c_3 n^3 + c_4 n^4}{n}\right) \quad (4)$$

where p is the pressure in Torr, n is the adsorbed amount in mmol g⁻¹, K is the Henry constant in mmol g⁻¹ Torr⁻¹ and c_i are the constants of the virial equation.

The free energy of desorption at a given temperature and pressure of the gas is obtained from the analytical integration of eq. (4):

$$G(T,p) = RT \int_0^p \frac{n}{p} dp = RT(n + \frac{1}{2}c_1n^2 + \frac{2}{3}c_2n^3 + \frac{3}{4}c_3n^4 + \frac{4}{5}c_4n^5) \quad (5)$$

The free energy of desorption is a function of temperature and pressure $G(T,p)$ and describes the minimum work (Gibbs free energy) that required to completely degas the adsorbent surface.

For a binary mixture of component i and j eq. (5) yields the individual pure loadings n_i^0 and n_j^0 at the same free energy of desorption:

$$G_i^0(n_i^0) = G_j^0(n_j^0) \quad (6)$$

The partial pressure of component i and j in an ideal adsorption mixture is given by the following equations:

$$py_i = p_i^0(n_i^0)x_i \quad (7)$$

$$py_j = p_j^0(n_j^0)x_j \quad (8)$$

where $y_i (=1-y_j)$ and $x_i (=1-x_j)$ is the molar fraction of component i in the gas phase and the adsorbed phase respectively and p_i^0, p_j^0 is the pure component pressure of i and j respectively. From eq. (6)-(8) and (3), the selectivity for the adsorbates i and j ($S_{i,j}$) and the total pressure (p) of the gas mixture were calculated from eq. (9) and eq. (10), respectively.

$$S_{ij} = \frac{x_i/y_i}{x_j/y_j} = \frac{p_j^0}{p_i^0} \quad (9)$$

$$p = \sum_i^j (p_i^o x_i) \quad (10)$$

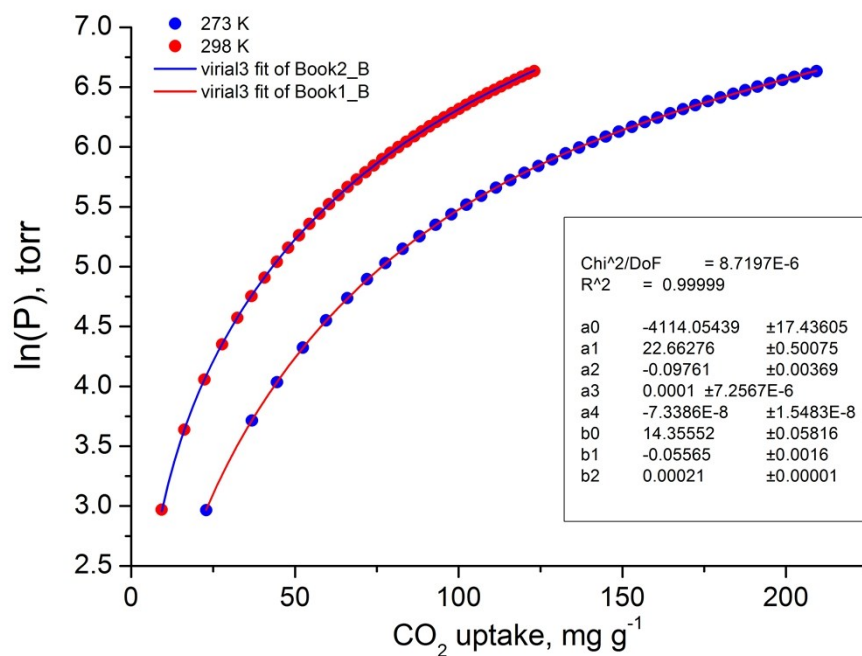


Figure S12. Virial type fitting of CO₂ adsorption isotherms of Cu-PEIP at 273 K and 298 K according to equation 1.

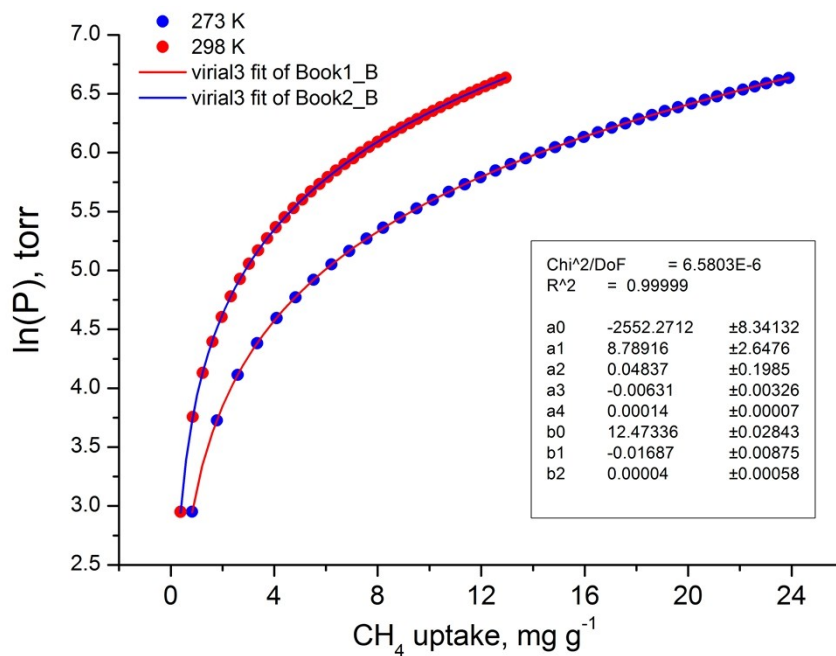


Figure S13. Virial type fitting of CH₄ adsorption isotherms of **Cu-PEIP** at 273 K and 298 K according to equation 1.

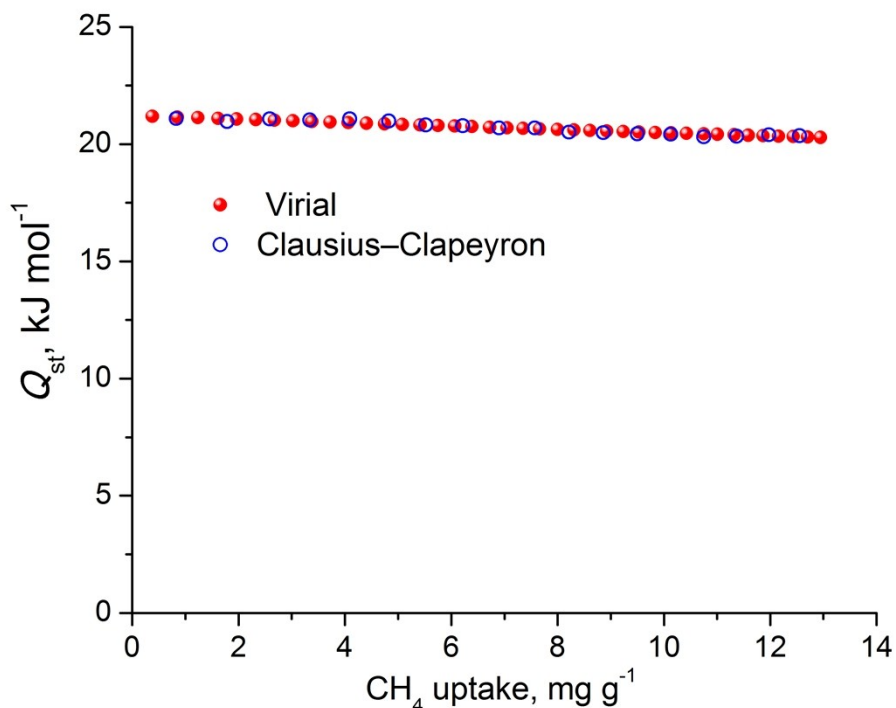


Figure S14. CH₄ isosteric heat of adsorption (Q_{st}) of **Cu-PEIP** as a function of surface coverage, calculated from a virial-type analysis. The corresponding Clausius-Clapeyron calculation is shown with the solid line.

Table S1. Comparison of **Cu-PEIP** with selected MOFs in terms of BET surface area, crystallographic density and total CH₄ uptake at 65 bar, working capacity (5-65 bar) at 298 K and isosteric heat of adsorption.

Material	BET area m ² g ⁻¹	Crystal density g cm ⁻³	Total gravimetric uptake g g ⁻¹	Total volumetric uptake cm ³ cm ⁻³	Gravimetric working capacity g g ⁻¹	Volumetric working capacity cm ³ cm ⁻³	Q_{st0} kJ mol ⁻¹
Cu-PEIP	1785	0.645	0.166	176	0.119	125	21.2
MAF-38	2022	0.761	0.247	263	0.176	187	21.6
Ni-MOF-74³	1350	1.195	0.148	251	0.077	129	21.4

UTSA-76⁴	2820	0.699	0.263	257	0.201	197	15.4
NU-111⁵	4930	0.409	0.360	205	0.313	177	14.2
HKUST-1⁶	1850	0.881	0.216	267	0.154	190	17
PCN-14⁶	2000	0.819	0.197	230	0.136	157	18.7
NU-1100⁶	4020	0.467	0.270	180	0.24	160	13.7

Table S2. Comparison of **Cu-PEIP** with selected MOFs in terms of total CH₄ uptake, and working capacity between 5-35 bar and 5-80 bar at 298 K.⁷

Material	Surface area, m ² g ⁻¹		Density, g cm ⁻³	Total uptake at 35 bar, cm ³ cm ⁻³	Total uptake at 80 bar, cm ³ cm ⁻³	Total uptake at 80 bar, g g ⁻¹	Workin g capacity at 35 bar, cm ³ cm ⁻³ 3	Workin g capacity at 80 bar, cm ³ cm ⁻³ 3	Workin g capacity at 80 bar, g g ⁻¹
	BET	Langm uir							
Cu-PEIP	1785	1814	0.762	150	187	0.176	99	136	0.129
MAF-38	2022	2229	0.761	226	273	0.256	150	197	0.185
MOF-520	3290	3930	0.586	162	231	0.282	125	194	0.237
Ni-MOF-74	1350	1438	1.195	230	267	0.160	115	152	0.091
HKUST-1	-	1977	0.881	225	272	0.221	153	200	0.162
PCN-14	-	2360	0.819	200	250	0.218	128	178	0.155

AX-21	-	4880	0.487	153	222	0.326	103	172	0.252
--------------	---	------	-------	-----	-----	-------	-----	-----	-------

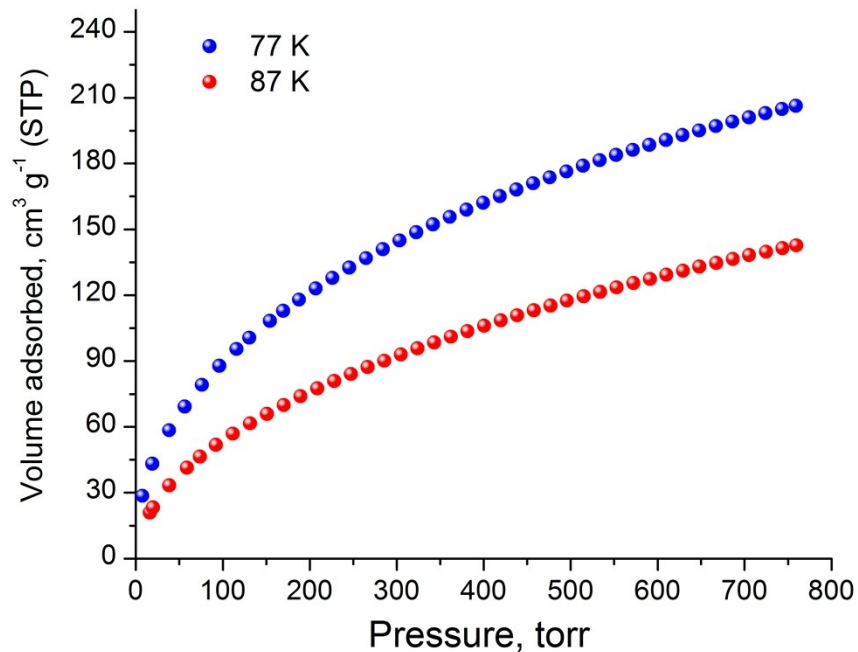


Figure S15. Hydrogen sorption isotherms of **Cu-PEIP** recorded at 77 K and 87 K.

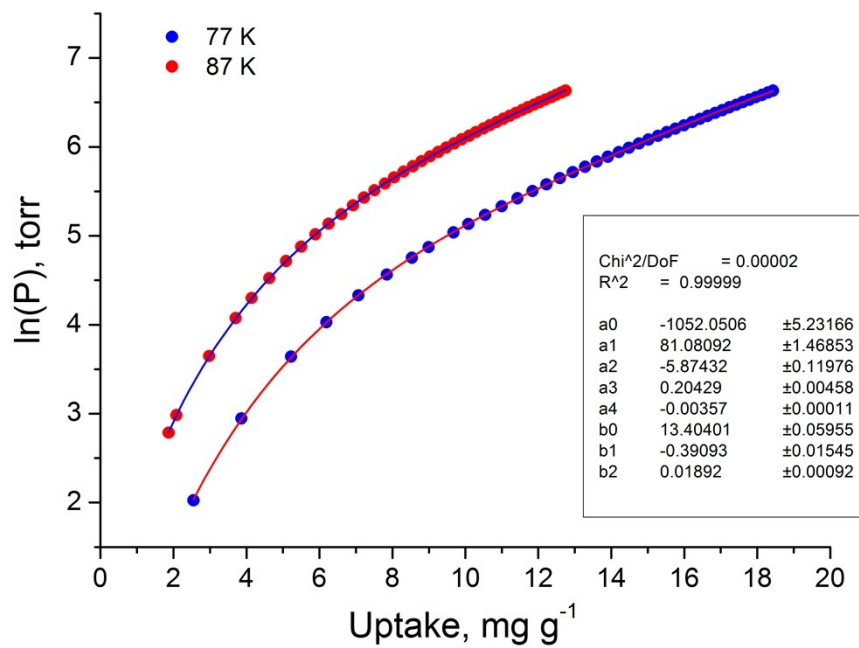


Figure S16. Virial type fitting of H₂ adsorption isotherms of **Cu-PEIP** at 77 K and 87 K according to equation 1.

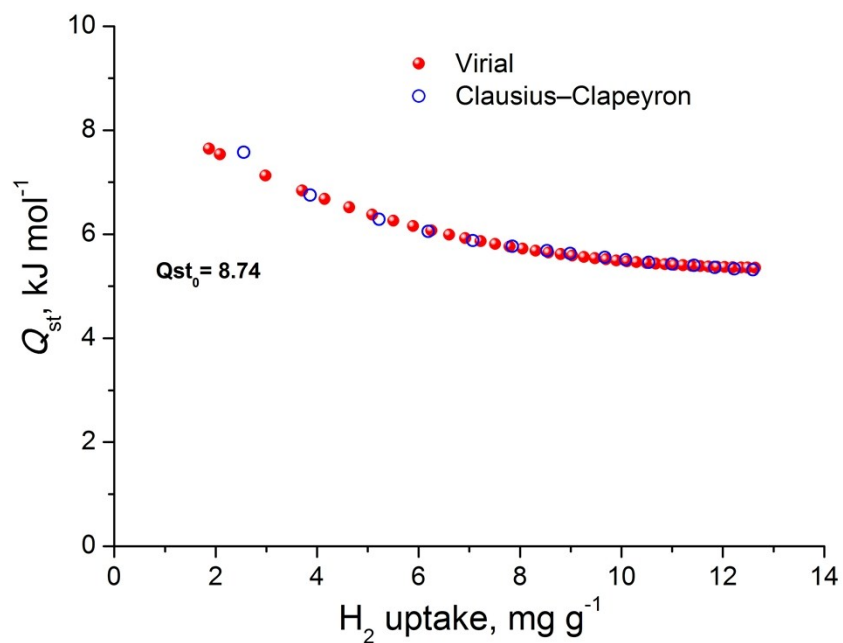


Figure S17. Hydrogen isosteric heat of adsorption (Q_{st}) of **Cu-PEIP** as a function of surface coverage, calculated from a virial-type analysis. The corresponding Clausius-Clapeyron calculation is shown with the solid line.

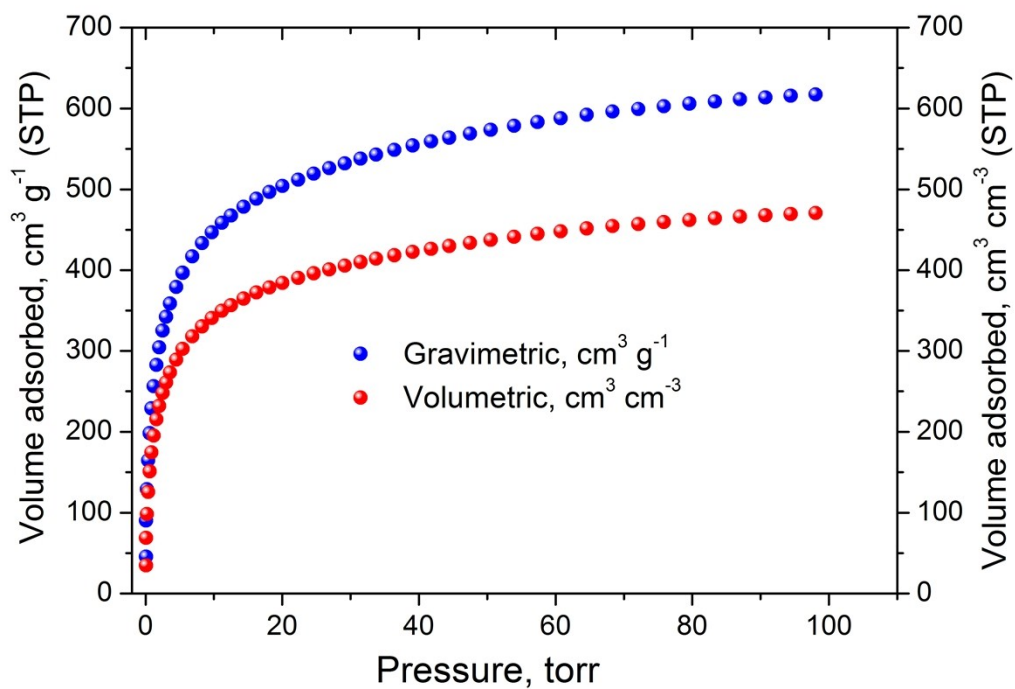


Figure S18. High pressure H₂ adsorption isotherm (up to 100 bar) of **Cu-PEIP** recorded at 77 K.

References

- 1** (a) L. Czepirski, J. Jagiello, *Chem. Eng. Sci.*, 1989, **44**, 797-801, (b) K. Sumida, D. L. Rogow, J. A. Mason, T. M. McDonald, E. D. Bloch, Z. R. Herm, T.-H. Bae, J. R. Long, *Chem. Rev.*, 2012, **112**, 724-781.
- 2** (a) A. L. Myers, J. M. Prausnitz, *AIChE J.*, 1965, **11**, 121-127. (b) Y. Bae, K. L. Mulfort, H. Frost, P. Ryan, S. Punnathanam, L. J. Broadbelt, J. T. Hupp, R. Q. Snurr, *Langmuir*, 2008, **24**, 8592-8598. (c) G.S. Armatas, M.G. Kanatzidis, *Nat. Mater.*, 2009, **8**, 217-222.
- 3** Y. Peng, V. Krungleviciute, I. Eryazici, J. T. Hupp, O. K. Farha, T. Yildirim, *J. Am. Chem. Soc.*, 2013, **135**, 11887-11894.
- 4** B. Li, H. Wen, H. Wang, H. Wu, M. Tyagi, T. Yildirim, W. Zhou, Chen B., *J. Am. Chem. Soc.*, 2014, **136**, 6207-6210.
- 5** Y. Peng, G. Srinivas, C. E. Wilmer, I. Eryazici, R.Q. Snurr, J. T. Hupp, T. Yildirim, O. K. Farha, *Chem. Commun.*, 2013, **49**, 2992-2994.
- 6** O. V. Gutov, W. Bury, D. A. Gomez-Gualdron, V. Krungleviciute, D. Fairen-Jimenez, J. E. Mondloch, A. A. Sarjeant, S. S. Al-Juaid, R. Q. Snurr, J. T. Hupp, T. Yildirim, O. K. Farha, *Chem. Eur. J.*, 2014, **20**, 12389-12393.
- 7** F. Gándara, H. Furukawa, S. Lee, O. M. Yaghi, *J. Am. Chem. Soc.*, 2014, **136**, 5271-5274.